CFD Letters

Journal homepage:
https://semarakilmu.com.my/journals/index.php/CFD_Letters/index
ISSN: 2180-1363

Dynamics of Tangent Hyperbolic Fluid Past a Semi-infinite Plate with the Significance of Joule Heating, Thermal Radiation and Soret-Dufour Mechanisms

Bidemi Olumide Falodun[1], Funmilayo Helen Oyelami[2,*], Gladys Tharapatla[3], Florence Dami Ayegbusi[4], Cletus Onwubuouya[1]

[1] Department of Computer Science/Mathematics, College of Natural and Applied Sciences, Novena University, Ogume, Delta State, Nigeria
[2] Department of Mathematical and Physical Sciences, Afe Babalola University, Ado EKiti, Nigeria
[3] Department of Mathematics, St Ann's College for Women, India
[4] Department of Mathematics and Statistics, First Technical University, Ibadan, Nigeria

ARTICLE INFO

Article history:
Received 5 June 2023
Received in revised form 8 July 2023
Accepted 12 August 2023
Available online 10 December 2023

Keywords:
Joule heating; Non-Newtonian liquid; Tangent hyperbolic liquid; Lorentz force; Spectral relaxation method

ABSTRACT

The present investigation concentrates on the unsteady flow of tangent hyperbolic liquid past a vertical plate under the influence of Lorentz force, Joule heating, and viscous dissipation. The mathematical modelling leads to nonlinear coupled partial differential equations (PDEs). Suitable non-dimensional quantities are applied to the governing PDEs to obtain dimensionless systems of equations. The transformed boundary layer PDEs are solved with the aid of the spectral relaxation method (SRM). The SRM employs the Gauss-Seidel techniques to linearize and decouple the system of nonlinear PDEs. The applied magnetic field acts as an opposition to the flow by producing the Lorentz force. The Weissenberg parameter, alongside the magnetic parameter, is observed to decline the velocity profile. An increment in thermal radiation parameter is observed to enhance the thickness of the hydrodynamic and thermal boundary layer. Therefore, the thermal condition and convective flow are improved with heat generation and thermal radiation in the flow phenomenon. This investigation is unique because it investigates the combined influence of Soret-Dufour and MHD, viscous dissipation, and Joule heating. This study plays a significant role in astrophysics, heat exchanger devices, MHD power generation, and geothermal energy extraction. When this study is compared to studies that have already been done, it agrees with those studies.

1. Introduction

The study of non-Newtonian liquids is more comprehensive when compared with Newtonian liquids. Non-Newtonian liquids possess variable viscosity due to the presence of an applied force. In analyzing non-Newtonian liquid behavior, many constitutive model equations have been used in the

* *Corresponding author.*
E-mail address: oyelamifunmilayo@abuad.edu.ng (Oyelami Funmilayo Helen)

https://doi.org/10.37934/cfdl.16.2.162183

literature. The tangent hyperbolic liquid is good enough to describe the phenomenon of shear thinning. The tangent hyperbolic fluid is a type of non-Newtonian fluid with shear-thinning characteristics. It has the same behaviour with pseudoplastic fluid with shear-thinning processes. This type of fluids undergo both steady and unsteady flow.

The analysis of tangent hyperbolic fluid as examined in this study flows over a semi-infinite vertical plate. Fluids of this type are blood, paint, ketchup, etc. Different physical properties are described in the literature to explain hyperbolic tangent fluid. The study of non-Newtonian fluids finds applications in bioengineering drilling operation and food processing. The flow of hyperbolic tangent liquid through a slanting, exponentially stretchy cylinder was investigated by Naseer *et al.,* [1]. Zakir and Gul [2] have studied MHD and slip restrictions in the Lie group for hyperbolic tangent fluids. Rao *et al.,* [3] use spectral techniques for solving the MHD boundary layer flow from a tangent hyperbolic liquid stretching cylinder. The nano-liquid flow of poisonous substances was studied by Mahdy and Hoshoudy [4]. The peristaltic flow of hyperbolic tangent liquid in three-dimensional and non-uniform media has been studied by Abbas *et al.,* [5]. The recent study of Falodun and Ige [6] examined the analysis of linear and quadratic multiple regression on the magneto-thermal and chemical reactions on the simultaneous flow of Casson-Williamson nanofluids.

The MHD flow of non-Newtonian liquids has gained attention in recent years because it is essential in physics and engineering. In heat alongside mass transport, the MHD nature of an electrically conducting liquid produces the Lorentz force. This force explains the usefulness of the imposed magnetism in controlling turbulence flow. The MHD finds numerous applications in electronics, chemical industries, power generations, MHD pumps and so on. The dynamics of MHD is the production of magnetic field due to fluid movement into a magnetic field. However, the MHD finds applications in nuclear power plants, MHD accelerators, gas turbines, geophysics, etc. Alao *et al.,* [7] explored the MHD flow of a chemically reacting liquid by utilizing spectral relaxation techniques. Bala [8] discussed the MHD flow of Casson liquid past a slanting penetrable stretchable surface. Hosseinzadeh *et al.,* [9] presented the impact of varying Lorentz forces on nano-liquid flow using an analytical approach. Ghadikolaei *et al.,* [10] give a detailed analysis of unsteady MHD Eyring-Powell flow in a stretchable medium. The flow of Powell-Eyring MHD nanomaterials has been elucidated by Hayat *et al.,* [11]. Shah *et al.,* [12] inspected MHD thin films on radiative Williamson liquid past a porous stretching sheet. Vijaya *et al.,* [13] discussed the unsteady flow of MHD Casson liquid with thermal radiation. Reddy and Krishna [14] discussed MHD micropolar liquid flow with Soret-Dufour's influence. Suneetha *et al.,* [15] studied heat and mass transport flows with MHD and thermal radiation. The recent study by Idowu and Falodun [16] explained the behavior of MHD while varying viscosity alongside thermal conductivity. Falodun *et al.,* [17] recently examined double-diffusive MHD viscous fluid flow in a porous medium in the presence of Cattaneo-Christov theories.

Thermal radiation and chemical reaction play a significant role in engineering and applied science. Its industrial applications are found in furnace design, glass production, plasma physics, propulsion systems, etc. The practical applications of thermal radiation is majorly in cooling system and surfactant applications to large scale heating. Thermal radiation is of great significance in scenario where the temperature is very high. It finds usefulness in oil-pipeline friction reduction. It is also applicable in the utilization of high-polymer additives to enhance petroleum pipe-lines flow which is very useful for commercial purposes. Fagbade *et al.,* [18] examined the effects of chemical reactions, magnetic fields, viscous dissipation, and thermophoresis on a mixed convective limit layer fluid flow. The effect of thermal radiation on heat transfer of liquid Casson with nanoparticles was investigated by Sobamowo [19]. Ganesh *et al.,* [20] investigated the heat transfer of thermal and magnetic fields of dusty hyperbolic tangent water. The MHD heat transfer of viscoelastic fluid was addressed by Fagbade *et al.,* [21]. Daniel [22] discussed laminar convective boundary layer slip flow over a flat plate

using the homotopy analysis method. Shehzad *et al.,* [23] investigated MHD tangent hyperbolic nanofluid with chemical reaction, viscous dissipation, and Joule heating effects. Shahzad *et al.,* [24] studied heat transfer analysis of MHD rotating flow of Fe_3O_4 nanoparticles through a stretchable surface. Hussain *et al.,* [25] examined the effects of viscous dissipation on MHD tangent hyperbolic fluid with convective boundary conditions. The recent study of Ayegbusi *et al.,* [26] elucidates the unsteady problem of MHD convective flow with thermal radiation and thermophoresis influence. Jabeen *et al.,* [27] studied chemically reacting MHD fluids in a porous channel with heat radiation. Anjum *et al.,* [28] studied the investigation of binary chemical reactions in magnetohydrodynamic nanofluid flow with double stratification. MHD Powell-Eyring dusty nanofluid flow due to stretching surface with heat flux boundary condition was investigated by Abo-Zaid *et al.,* [29]. Yadav and Verma [30] elucidated the analysis of immiscible Newtonian and non-Newtonian micropolar fluid flows through a porous cylindrical pipe enclosing a cavity.

Hussain *et al.,* [31] explored the computational investigation of the combined impact of nonlinear radiation and magnetic field on three-dimensional rotational nanofluid flow across a stretching surface. Dawar *et al.,* [32] studied magnetized and non-magnetized Casson fluid flow with gyrotactic microorganisms over a stratified stretching cylinder. Falodun *et al.,* [33] recently examined the positive and negative Soret and Dufour mechanisms in unsteady heat and mass transfer flow. In another study by Falodun *et al.,* [34], MHD heat and mass transfer of Casson fluid flow past a semi-infinite vertical plate with thermophoresis are considered. The significance of Lorentz force and thermal radiation has attracted many researchers in recent time due to their industrial applications in engineering and applied sciences. The Lorentz force finds usefulness in the control of turbulent flow in aerospace engineering. Thermal radiation is very useful in flow phenomenon where the temperature is very high and in the conversion of thermal energy. Hussain *et al.,* [35] studied heat transport investigation of magneto-hydrodynamics (SWCNT-MWCNT) hybrid nanofluid under the thermal radiation regime. In another study, Hussain *et al.,* [36] gave detailed explanation on three-dimensional water-based magneto-hydrodynamic rotating nanofluid flow using numerical approach.

Based on the aforementioned published works, little or no work has examined the effects of Lorentz force, Joule heating, and viscous dissipation on the unsteady flow of tangent hyperbolic liquid past a vertical plate. Keeping this in mind, the dynamics of unsteady tangent hyperbolic fluid flow past a semi-infinite vertical plate is addressed in this paper. The study of Alao *et al.,* (2016) was Newtonian, it was extended in the present study to examine the flow of Tangent hyperbolic non-Newtonian fluid. Also, the motivation to this study was to examine the significance of Joule heating, viscous dissipation, and Soret-Dufour mechanisms on the dynamics of Tangent hyperbolic fluid. The study of this type has not been examined in literature before based on our knowledge. Tangent hyperbolic fluid is a non-Newtonian fluid in which the constitutive equation is valid for low and high shear rates. The fluid under investigation shows the characteristics of the relaxation time and the retardation time. In experiments, the viscosity of non-Newtonian fluids is independent of shear, but average stress differences can still be seen. The novelty of this paper is the consideration of the combined effects of the Soret-Dufour mechanism on the tangent hyperbolic fluid in the presence of heat generation and chemical reactions. The analysis in this paper is of practical applications in science and engineering, such as the Lorentz force in MHD accelerators, chemical catalytic reactors, Soret in isotope separation, etc. Using SRM, the flow PDEs are solved numerically, and the effects of the parameters that are found are shown in graphs.

2. Flow Analysis

Consider the laminar, unsteady, two-dimensional flow of MHD tangent hyperbolic liquid past a semi-infinite vertical porous plate with viscous dissipation and thermal radiation. The plate is assumed to be infinite in x^* direction while the y^*-direction normal to the plate (see Figure 1). The movement of the upward plate is assumed only towards the y^*-axis. Hence the derivative $\frac{\partial u^*}{\partial x^*}$ is forgone. Initially, when the fluid is set into motion, the time $t^* \leq 0$ both the plate alongside the fluid maintains uniform temperature. The plate is considered to be vertically upward. As the plate moves vertically upward, the effect is noticed towards the y^*-axis. Hence, any function with respect to x^*-axis is neglected in the model (see Alao *et al.,* (2016), Falodun *et al.,* (2018)). The vertical component has effect on the flow phenomenon due to the thermal buoyancy and mass buoyancy considered in this study. The x^* −axis was neglected in the governing equations because the moving semi-infinite plate moves vertically towards the horizontal y^*-axis. Also, terms involving x^*-axis is neglected in the heat flux because it is considered such that $\frac{\partial q_r}{\partial y*} \gg \frac{\partial q_r}{\partial x*}$. Hence, the radiative heat flux in the x^*-direction $\frac{\partial q_r}{\partial x*}$ is negligible. Therefore, $\frac{\partial q_r}{\partial y*}$ dominate the flow. Figure 1 describes the physical phenomenon of the tangent hyperbolic fluid flow within the boundary layers. The magnetic field strength is observed to be in opposite direction as shown in Figure 1. The flow direction as shown in Figure 1 is vertically upward.

In view of this, thermal radiation along with heat generation is taking into account. A magnetism of uniform strength (B_0) is transversely imposed to both plate and flow direction. The magnetic Reynolds number is assumed to be small such that induced magnetic field is forgone. The level of species is assumed to be high such that Soret-Dufour effects are considered. Following Hussain *et al.,* [25] and the definition of Cauchy stress tensor τ as:

$$\tau = -pI + S \tag{1}$$

The constitutive analysis of extra tensor S of tangent hyperbolic liquid as described by Hussain *et al.,* [25], gives;

$$S = [\mu_\infty + (\mu_0 + \mu_\infty)\tanh(\Gamma\dot{\gamma})^n]A_1 \tag{2}$$

μ_∞ signifies shear rate viscosity, μ_0 signifies zero shear rate viscosity, Γ signifies dependent material constant, n signifies the power-law index, A_1 signifies the first tensor Rivlin-Erickson. From the above, $\dot{\gamma}$ gives:

$$\dot{\gamma} = \sqrt{\frac{1}{2}tr(A_1^2)} \tag{3}$$

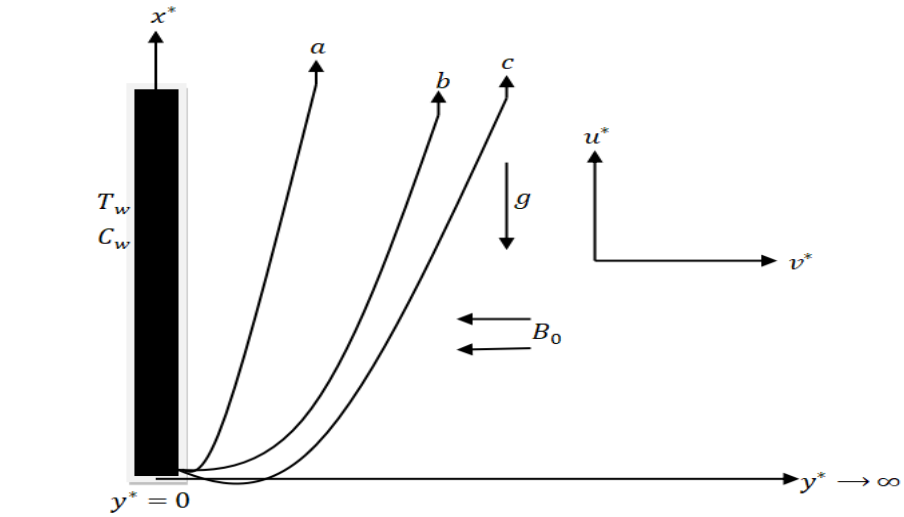

a =Momentum Boundary Layer

b =Thermal Boundary Layer

c =Concentration Boundary Layer

Fig. 1. Physical geometry

For the sake of simplicity, consider $\mu_\infty = 0$ in Eq. (2) and since tangent hyperbolic liquid explains shear-thinning analysis. Therefore, $\Gamma\dot{\gamma} < 1$. Utilizing the above simplifications on Eq. (2) to obtain:

$$S = \mu_0[(\Gamma\dot{\gamma})^n]A_1 \tag{4}$$

Simplifying the above to obtain;

$$S = \mu_0[1+n(\Gamma\dot{\gamma}-1)]A_1 \tag{5}$$

Under the assumptions above and following Alao *et al.,* [7] the flow equations along with the boundary constraints are:

$$\frac{\partial v^*}{\partial y^*} = 0 \tag{6}$$

$$\frac{\partial u^*}{\partial t^*} + v^*\frac{\partial u^*}{\partial y^*} = \nu(1-n)\frac{\partial^2 u^*}{\partial y^{*2}} + \sqrt{2}\nu n\Gamma\frac{\partial u^*}{\partial y^*}\frac{\partial^2 u^*}{\partial y^{*2}} - \frac{\sigma B_0^2}{\rho}u^* + g\beta_t(T-T_\infty) + g\beta_c(C-C_\infty) \tag{7}$$

$$\frac{\partial T}{\partial t^*} + v^*\frac{\partial T}{\partial y^*} = \alpha\frac{\partial^2 T}{\partial y^{*2}} + \frac{\nu}{c_p}\left(\frac{\partial u^*}{\partial y^*}\right)^2 - \frac{1}{\rho c_p}\frac{\partial q_r}{\partial y^*} + \frac{Q_0}{\rho c_p}(T-T_\infty) + \frac{Dk_T}{c_s c_p}\frac{\partial^2 C}{\partial y^{*2}} + \frac{\sigma B_0^2}{\rho c_p}u^2 \tag{8}$$

$$\frac{\partial C}{\partial t^*} + v^*\frac{\partial C}{\partial y^*} = D\frac{\partial^2 C}{\partial y^{*2}} + \frac{Dk_T}{T_m}\frac{\partial^2 T}{\partial y^{*2}} - K_r(C-C_\infty) \tag{9}$$

subject to the constraints [Alao *et al.,* [7]]:

$$u = U_0, T = T_w + \psi(T_w - T_\infty)e^{n^{**}t}, C = C_w + \psi(C_w - C_\infty)e^{n^{**}t}, \ at \ \ y^* = 0 \tag{10}$$

$$u^* \to 0, T \to T_\infty, C \to C_\infty, \ as \ \ y^* \to \infty \tag{11}$$

We obtain the suction velocity normal to the plate by integrating both sides of Eq. (1). Following the analysis presented by Idowu and Falodun [37], the wall suction velocity is a function of constant and time-dependent given as;

$$v^* = -v_0\left(1 + \xi A e^{n^* t^*}\right) \tag{12}$$

In this analysis, the radiative heat flux was assumed to be $\frac{\partial q_r}{\partial y^*} >> \frac{\partial q_r}{\partial x^*}$ since the heat flux diverges only towards y^*-direction. Hence, the heat flux $\frac{\partial q_r}{\partial y^*}$ dominates the fluid flow. Considering that, the difference in temperature throughout the flow is small in a way that T^4 is evaluated as a linear function of the ambient temperature, T_∞. Simplifying T^4 in Taylor's approach in T_∞ and forgone terms of higher-order to obtain:

$$T^4 \approx 4T_\infty^3 T - 3T_\infty^4 \tag{13}$$

Utilizing Rosse; and approximation, the heat flux in terms of y^* gives

$$q_r = -\frac{4\sigma_0}{3ke}\frac{\partial T^4}{\partial y^*} \tag{14}$$

Here σ_0 signifies Stefan-Boltzmann constant and ke signifies mean absorption coefficient. Since the Rosseland approximation was utilized in this analysis, the tangent hyperbolic liquid is assumed to be optically thick liquids. Linearizing the (9) above and utilizing the outcome on the energy equation to obtain;

$$\frac{\partial T}{\partial t^*} + v^* \frac{\partial T}{\partial y^*} = \alpha \frac{\partial^2 T}{\partial y^{*2}} + \frac{\nu}{c_p}\left(\frac{\partial u^*}{\partial y^*}\right)^2 + \frac{16\sigma_0}{3\rho c_p ke} T_\infty^3 \frac{\partial^2 T}{\partial y^{*2}} + \frac{Q_0}{\rho c_p}(T - T_\infty) + \frac{Dk_T}{c_s c_p}\frac{\partial^2 C}{\partial y^{*2}} + \frac{\sigma B_0^2}{\rho c_p}u^2 \tag{15}$$

The flow governing equations are written in a dimensionless form using

$$u = \frac{u^*}{u_0}, y = \frac{v_0^2 y^*}{\nu}, t = \frac{v_0^2 t^*}{\nu}, n = \frac{\nu n^*}{v_0^2}, \theta = \frac{T - T_\infty}{T_w - T_\infty}, \phi = \frac{C - C_\infty}{C_w - C_\infty} \tag{16}$$

Utilizing the above quantities on the flow equations with the boundary constraints to obtain the following flow PDEs:

$$\frac{\partial u}{\partial t} - (1 + \xi A e^{nt})\frac{\partial u}{\partial y} = (1 - n)\frac{\partial^2 u}{\partial y^2} + nWe\frac{\partial u}{\partial y}\frac{\partial^2 u}{\partial y^2} - M^2 u + Gr\theta + Gm\phi \tag{17}$$

$$\frac{\partial\theta}{\partial t}-(1+\xi Ae^{nt})\frac{\partial\theta}{\partial y}=\left(\frac{1+R}{Pr}\right)\frac{\partial^2\theta}{\partial y^2}+Ec\left(\frac{\partial u}{\partial y}\right)^2+Du\frac{\partial^2\phi}{\partial y^2}+\delta_x\theta+M^2Ecu^2 \tag{18}$$

$$\frac{\partial\phi}{\partial t}-(1+\xi Ae^{nt})\frac{\partial\phi}{\partial y}=\left(\frac{1}{Sc}\right)\frac{\partial^2\phi}{\partial y^2}-Kr\phi+So\frac{\partial^2\theta}{\partial y^2} \tag{19}$$

Subject to:

$$u=1,\theta=1+\xi e^{nt},\phi=1+\xi e^{nt}\qquad at\quad y=0 \tag{20}$$

$$u\to 0,\theta\to 0,\phi\to 0,\ as\ \ y\to\infty \tag{21}$$

Note that $We=\frac{\sqrt{2}u_0v_0^2\Gamma}{\nu}$, $Gm=\frac{g\beta_c\nu(C_w-C_\infty)}{u_0v_0^2}$, $Ec=\frac{u_0^2}{c_p(T_w-T_\infty)}$, $Sc=\frac{\nu}{D}$, $M=\frac{\sigma B_0^2\nu}{\rho v_0^2}$, $R=\frac{16\sigma_0T_\infty^3}{3k_eK}$, $Du=\frac{Dk_T(C_w-C_\infty)}{c_sc_p\nu(T_w-T_\infty)}$, $K_r=\frac{k_r\nu}{v_0^2}$, $Gr=\frac{g\beta_t\nu(T_w-T_\infty)}{u_0v_0^2}$, $Pr=\frac{\nu\rho c_p}{k}=\frac{\nu}{\alpha}$, $\delta_x=\frac{Q_0\nu}{\rho c_pv_0^2}$, $So=\frac{Dk_T(T_w-T_\infty)}{T_m\nu(C_w-C_\infty)}$

where $We, Gm, Ec, Sc, M, R, Du, Kr, Gr, Pr, \delta_x$ and So are Weissenberg number, mass Grahof number, Eckert number, Schmidt number, magnetic term, thermal radiation parameter, Dufour term, chemical reaction parameter, thermal Grashof number, Prandtl number, heat generation parameter and Soret term. The engineering quantities of curiosity are defined as follows:

Skin friction $C_f=\frac{\tau_w'}{\rho U_0V_0}=\left(\frac{\partial u}{\partial y}\right)|_{y=0}$

Nusselt number $\mathrm{Nu}=\frac{\mathrm{q_w}}{\mathrm{k(T_w-T_\infty)}}$

Sherwood number $(Sh)=\frac{-Dq_m}{(C_w-C_\infty)}$

Where;

$$q_w=-k\left(\frac{\partial T}{\partial y}|_{y=0}-\frac{4\sigma_0}{3ke}\left(\frac{\partial T^4}{\partial y}\right)|_{y=0}\right),S_w=\left(\frac{\partial C}{\partial y}\right)_{y=0}$$

By utilizing dimensional quantities stated in Eq. (16), the physical quantities are resolved to be;

$NuRe_x^{-1}=-\left(\frac{\partial\theta}{\partial y}-\frac{R}{Pr}\frac{\partial^2\theta}{\partial y^2}\right)_{y=0}$ is the rate of heat transfer

$ShRe_x^{-1}=-\left(\frac{\partial\phi}{\partial y}\right)_{y=0}$ is the rate of mass transfer

Where $Re_x=\frac{V_0x}{\nu}$ denote the local Reynolds number

3. Spectral Relaxation Technique

The transformed PDEs are solved numerically utilizing SRM. SRM is an iterative approach that uses the Gauss-seidel type's relaxation approach to decouple and linearize the coupled equations. The linearized equations will be discretized and solved by employing the Chebyshev pseudo-spectral method (Motsa, [38]). The degree of iteration was facilitated on all linear terms at the current iteration noted, while nonlinear terms are assumed to be known from the previous iteration noted. The SRM is a powerful tool in solving PDEs. It helps in decoupling and linearizing coupled or nonlinear equations. The SRM played a significance role in solving non-Newtonian complex equations. The basic steps of the spectral approach are:

i. First, decouple the nonlinear equations and linearize them using Gauss-Siedel techniques;
ii. The linearized equations were further discretized, and
iii. The discretized equations are solved iteratively by utilizing the Chebyshev pseudo-spectral technique.

Using the SRM on the nonlinear coupled PDEs (12) - (14) leads to:

$$\frac{\partial u_{r+1}}{\partial t} = (1+\xi A e^{nt})\frac{\partial u_{r+1}}{\partial y} + (1-n)\frac{\partial^2 u_{r+1}}{\partial y^2} + nWe\frac{\partial u_{r+1}}{\partial y}\frac{\partial^2 u_{r+1}}{\partial y^2} - M^2 u_{r+1} + Gr\theta_r + Gm\phi_r \quad (22)$$

$$\frac{\partial \theta_{r+1}}{\partial t} = (1+\xi A e^{nt})\frac{\partial \theta_{r+1}}{\partial y} + \left(\frac{1+R}{Pr}\right)\frac{\partial^2 \theta_{r+1}}{\partial y^2} + Ec\left(\frac{\partial u_{r+1}}{\partial y}\right)^2 + Du\frac{\partial^2 \phi_r}{\partial y^2} + \delta_x\theta_{r+1} + M^2 Ecu_{r+1}^2 \quad (23)$$

$$Sc\frac{\partial \phi_{r+1}}{\partial t} = Sc(1+\xi A e^{nt})\frac{\partial \phi_{r+1}}{\partial y} + \frac{\partial^2 \phi_{r+1}}{\partial y^2} - Sck_r^2\phi_{r+1} + ScSr\frac{\partial^2 \theta_{r+1}}{\partial y^2} \quad (24)$$

Subject to

$$u_{r+1}(0,t) = 1, \theta_{r+1}(0,t) = 1+\xi e^{nt}, \phi_{r+1}(0,t) = 1+\xi e^{nt} \quad (25)$$

$$u_{r+1}(\infty,t) = 0, \theta_{r+1}(\infty,t) = 0, \phi_{r+1}(\infty,t) = 0 \quad (26)$$

Defining coefficient parameters from the above equations as:

$$\gamma = (1+\xi A e^{nt}), \gamma_{0,r} = nWe\frac{\partial u_{r+1}}{\partial y}, \gamma_{1,r} = Gr\theta_r + Gm\phi_r, \gamma_{2,r} = \left(\frac{1+R}{Pr}\right)$$

$$\gamma_{3,r} = Ec\left(\frac{\partial u_{r+1}}{\partial y}\right)^2, \gamma_{4,r} = Du\frac{\partial^2 \phi_r}{\partial y^2}, \gamma_{5,r} = M^2 Ecu_{r+1}^2, \gamma_{6,r} = So\frac{\partial^2 \theta_{r+1}}{\partial y^2} \quad (27)$$

Putting the coefficient parameters above into (17)-(19) to obtain;

$$\frac{\partial u_{r+1}}{\partial t} = \gamma\frac{\partial u_{r+1}}{\partial y} + (1-n)\frac{\partial^2 u_{r+1}}{\partial y^2} + \gamma_{0,r}\frac{\partial^2 u_{r+1}}{\partial y^2} - M^2 u_{r+1} + \gamma_{1,r} \quad (28)$$

$$\frac{\partial \theta_{r+1}}{\partial t} = \gamma \frac{\partial \theta_{r+1}}{\partial y} + \gamma_{2,r} \frac{\partial^2 \theta_{r+1}}{\partial y^2} + \gamma_{3,r} + \gamma_{4,r} + \delta_x \theta_{r+1} + \gamma_{5,r} \tag{29}$$

$$\frac{\partial \phi_{r+1}}{\partial t} = \gamma \frac{\partial \phi_{r+1}}{\partial y} + \frac{1}{Sc} \frac{\partial^2 \phi_{r+1}}{\partial y^2} - Kr\phi_{r+1} + \gamma_{6,r} \tag{30}$$

Subject to

$$u_{r+1}(0,t) = 1, \theta_{r+1}(0,t) = 1 + \xi e^{nt}, \phi_{r+1}(0,t) = 1 + \xi e^{nt} \quad at \;\; y = 0 \tag{31}$$

$$u_{r+1}(\infty,t) = 0, \theta_{r+1}(\infty,t) = 0, \phi_{r+1}(\infty,t) = 0, \text{at } y \to \infty \tag{32}$$

The Gauss-Lobatto points given as follows are used to define the unknown functions.

$$\xi_j = cos\frac{\pi j}{N}, \;\; j = 0,1,2,...,N; \; 1 \le \xi \le -1 \tag{33}$$

Here, it N signifies the collocation points number. The physical region domain $[0,\infty]$ is transformed to $[-1,1]$ change the present region. Thus, the problem is solved in this way: The transformation defined below is used to map the interval.

$$\frac{\eta}{L} = \frac{\xi + 1}{2}, \; -1 \le \xi \le 1 \tag{34}$$

Here L signifies the scaling term utilized in simplifying the boundary constraint at infinity. The initial simplification for solving Eq. (23)-(25) are gotten at $y = 0$ and are considered subject to the boundary constraints (20) and (21). Hence, $u_0(y,t), \theta_0(y,t)$ and $\phi_0(y,t)$ are chosen as;

$$u_0(y,t) = e^{-y}, \theta_0(y,t) = \phi_0(y,t) = e^{-y} + \xi e^{nt} \tag{35}$$

The systematic Eq. (28)-(30) would be solved using the iterative technique for unknown functions right from the initial approximations in Eq. (35). The schemes Eq. (28), (29), and (30) are iteratively solved for $u_{r+1}(y,t), \theta_{r+1}(y,t)$ and $\phi_{r+1}(y,t)$ as $r = 0,1,2$. In the Eq. (28)-(30), we discretized by utilizing the Chebyshev spectral collocation approach y while the implicit finite difference technique is utilized in the direction of t. The finite difference scheme was employed at the mid-point between t^{n+1} and t^n. The mid-point is defined as

$$t^{n+\frac{1}{2}} = \frac{t^{n+1} + t^n}{2} \tag{36}$$

Thus utilizing the centering about $t^{n+\frac{1}{2}}$ to the functions, say $u(y,t), \theta(y,t)$ and $\phi(y,t)$ alongside associated derivative to obtain;

$$u(y_j,t^{n+\frac{1}{2}}) = u_j^{n+\frac{1}{2}} = \frac{u_j^{n+1}+u_j^n}{2}, \left(\frac{\partial u}{\partial t}\right)^{n+\frac{1}{2}} = \frac{u_j^{n+1}-u_j^n}{\Delta t} \tag{37}$$

$$\theta(y_j,t^{n+\frac{1}{2}}) = \theta_j^{n+\frac{1}{2}} = \frac{\theta_j^{n+1}+\theta_j^n}{2}, \left(\frac{\partial \theta}{\partial t}\right)^{n+\frac{1}{2}} = \frac{\theta_j^{n+1}-\theta_j^n}{\Delta t} \tag{38}$$

$$\phi(y_j,t^{n+\frac{1}{2}}) = \phi_j^{n+\frac{1}{2}} = \frac{\phi_j^{n+1}+\phi_j^n}{2}, \left(\frac{\partial \phi}{\partial t}\right)^{n+\frac{1}{2}} = \frac{\phi_j^{n+1}-\phi_j^n}{\Delta t} \tag{39}$$

The spectral collocation approach requires the implementation of a differentiation matrix D to evaluate the derivatives of variables unknown gave as

$$\frac{d^r u}{dy^r} = \sum_{k=0}^{N} D_{ik}^r u(\xi_k) = D^r u, \ \ i = 0,1,...N \tag{40}$$

$$\frac{d^r \theta}{dy^r} = \sum_{k=0}^{N} D_{ik}^r \theta(\xi_k) = D^r \theta, \ \ i = 0,1,...N \tag{41}$$

$$\frac{d^r \phi}{dy^r} = \sum_{k=0}^{N} D_{ik}^r \phi(\xi_k) = D^r \phi, \ \ i = 0,1,...N \tag{42}$$

Figure 2 shows the Flow diagram of the present solution techniques.

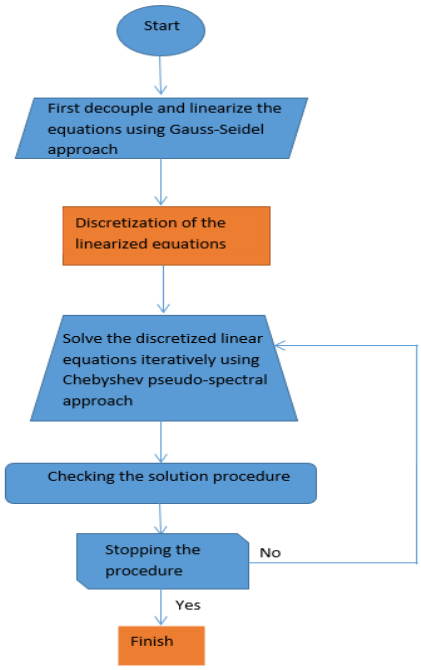

Fig. 2. Flow diagram of the present solution techniques (see Falodun *et al.,* [17])

The Chebyshev spectral collocation approach was first used on Eq. (28) - (30), followed by the finite differences.

$$\frac{du_{r+1}}{dt} = [\gamma D + (1-n)D^2 + \gamma_{0,r}D^2 - M^2]u_{r+1} + \gamma_{1,r} \tag{43}$$

$$\frac{d\theta_{r+1}}{dt} = [\gamma D + \gamma_{2,r}D^2 + \delta_x]\theta_{r+1} + \gamma_{3,r} + \gamma_{4,r} + \gamma_{5,r} \tag{44}$$

$$\frac{d\phi_{r+1}}{dt} = [\gamma D + \frac{1}{Sc}D^2 - Kr]\phi_{r+1} + \gamma_{6,r} \tag{45}$$

Subject to Eq. (20) and (21) where

$$u_{r+1} = \begin{bmatrix} u_{r+1}(x_0,t) \\ u_{r+1}(x_1,t) \\ \vdots \\ u_{r+1}(x_{N_{x-1}},t) \\ u_{r+1}(x_{N_x},t) \end{bmatrix}, \gamma_{0,r} = \begin{bmatrix} \gamma_{0,r}(x_0,t) & & & & \\ & \gamma_{0,r}(x_1,t) & & & \\ & & \ddots & & \\ & & & \ddots & \\ & & & & \gamma_{0,r}(x_{N_x},t) \end{bmatrix} \tag{46}$$

$$\theta_{r+1} = \begin{bmatrix} \theta_{r+1}(x_0,t) \\ \theta_{r+1}(x_1,t) \\ \vdots \\ \theta_{r+1}(x_{N_{x-1}},t) \\ \theta_{r+1}(x_{N_x},t) \end{bmatrix}, \ \phi_{r+1} = \begin{bmatrix} \phi_{r+1}(x_0,t) \\ \phi_{r+1}(x_1,t) \\ \vdots \\ \phi_{r+1}(x_{N_{x-1}},t) \\ \phi_{r+1}(x_{N_x},t) \end{bmatrix} \tag{47}$$

From Eq. (40)-(42), the following scheme is obtained

$$M_1 u_{r+1}^{n+1} = M_2 u_{r+1}^{n} + K_1 \tag{48}$$

$$M_3 \theta_{r+1}^{n+1} = M_4 \theta_{r+1}^{n} + K_2 \tag{49}$$

$$M_5 \phi_{r+1}^{n+1} = M_6 \phi_{r+1}^{n} + K_3 \tag{50}$$

Subject to the following initial and boundary conditions:

$$u_{r+1}(xN_x, t^n) = \theta_{r+1}(xN_x, t^n) = \phi_{r+1}(xN_x, t^n) = 0 \tag{51}$$

$$u_{r+1}(x_0, t^n) = 1, \theta_{r+1}(x_0, t^n) = \phi_{r+1}(x_0, t^n) = 1 + \xi e^{nt}, \ n = 1,2,\ldots \tag{52}$$

$$u_{r+1}(y_j, 0) = e^{-y_j}, \theta_{r+1}(y_j, 0) = \phi_{r+1}(y_j, 0) = e^{-y_j} + \xi e^{nt} \tag{53}$$

The above matrices are defined as;

$$M_1 = \frac{1}{2} - \frac{(\gamma D + (1-n)D^2 + \gamma_{0,r}D^2 - M^2)}{2}, M_2 = \frac{1}{2} + \frac{(\gamma D + (1-n)D^2 + \gamma_{0,r}D^2 - M^2)}{2}$$

$$M_3 = \frac{1}{2} - \frac{(\gamma D + \gamma_{2,r} D^2 + \delta_x)}{2}, M_4 = \frac{1}{2} + \frac{(\gamma D + \gamma_{2,r} D^2 + \delta_x)}{2}$$

$$M_5 = \frac{1}{2} - \frac{\gamma D + \frac{1}{Sc} D^2 - Kr}{2}, M_6 = \frac{1}{2} + \frac{\gamma D + \frac{1}{Sc} D^2 - Kr}{2}$$

4. Results and Discussions

The equations that govern the fluid model are solved numerically via SRM. The procedure of this iterative numerical method (SRM) is illustrated in Figure 2. The effects of physical flow parameters on dimensionless concentration, velocity, and temperature are presented in graphs and tables. The default values of parameters are set to be We=M=1, So=0.6, Du=0.9, R=0.5, Sc=0.61, Pr=7.0, Gr=2Gm=2, kr=0.3 and Ec=0.1.

Figure 3 depicts the effect of the Weissenberg number (We) on velocity plot. It is noted in Figure 3 that an increase in We lowers the fluid motion by decelerating the velocity profile. The Tangent hyperbolic fluid possess a shear-thinning characteristics. It has the same behaviour with pseudoplastic fluid with shear-thinning processes. A higher value of We decreases the velocity because the Tangent hyperbolic fluid is a high viscous fluid. This shows a decrease in the hydrodynamics boundary layer thickness. The thickness of the layer reduces as a result of high viscosity which brings resistance to the fluid flow phenomenon. The Weissenberg number is equivalent to relaxation time. Therefore, we will enhance the relaxation time to allow more significant resistance to the motion of the fluid by reducing the momentum layer thickness. On temperature and concentration, they are found to be negligible, with no effect on the profiles. The effect of the Soret term (So) on the temperature, velocity, and concentration is depicted in Figure 4. An increase in the values of So is observed to enhance the velocity alongside the concentration plot. This is owing to greater thermal diffusion as the values of So are raised. It is worth noting that a positive Soret term leads to a stabilized effect. The moment So > 0, a hike in temperature will lead to a degeneration in density as well as the mass fraction of species concentration. It is referred to as a “cooperative solute” and a “thermal gradient” as the solute spreads to cold regions. On the other hand, when So, a hike in temperature results in a competitive solutal and thermal gradient as the solute spreads to warmer regions. Hence, an elevation is noticed on the velocity and concentration plots while the effect of So is negligible on the temperature plot. Higher So leads to an increase in both hydrodynamic and concentration boundary layer thickness. The outcomes in Figure 4 are in good agreement with the outcomes of Idowu and Falodun (2019) in the absence of the viscoelastic parameter.

The Impact of the Dufour term (Du) on the temperature, velocity, and concentration plot is illustrated in Figure 5. The Dufour term portrays the impact of concentration gradients on the temperature, as noted in Eq. (8). The Dufour number explains the contribution of concentration gradients to the thermal energy flux which exists within the flow. It is a dimensionless number employed in examining thermodiffusion equivalent to elevation in enthalpy of a unit mass during isothermal mass transfer. It assists the flow and also tends to boost thermal energy within the layers. As depicted in Figure 5, a considerable value of Du is detected to elevate the momentum and the thermal layer thickness. Hence, an increase in velocity and temperature plots is noticeable for a considerable value of Du. On the other hand, the effect of Du on the concentration plot is negligible, as shown in Figure 5.

Figure 6 depicts the impact of the magnetic term (M) on the concentration, velocity, and temperature plots. The degeneration in the velocity profile is noticeable for a considerable value of M, while the effect of M is neglected on the temperature and concentration plots. This is because the Lorentz force is generated as the magnetic field is imposed in the direction of flow. The Lorentz force is the force exerted on charged particles moving with the fluid velocity through both electric and magnetic fields. This force acts against liquid velocity and thereby degenerates the velocity and the momentum layer thickness. Figure 7 portrays the thermal radiation parameter I impact on the velocity, concentration, and temperature plots. An increase in velocity and temperature is detected as the values of R increase. Physically, the thermal energy has a significant effect on the flow due to an increase in R. As a result of this, radiation has a significant impact on the flow when and. Hence, an increase in the thermal condition, temperature, and thermal layer are noticeable for R considerable value. The thermal radiation plays a significance role in a scenario where the temperature is very high. Hence, at a very high values of R the temperature within such environment increases drastically.

The Schmidt number (Sc) effect on ”eloc’ty, temperature, and concentration plot is depicted in Figure 8. A considerable value of Sc causes degeneration of the velocity and concentration plots. Sc is the quotient of kinematic viscosity to fluid mass diffusivity. Practically, it signifies higher Sc and vice versa. The rate of mass transport degenerates due to the effects of concentration buoyancy and leads to a decrease in the concentration plot. Hence, the outcomes in Figure 8 show higher viscosities compared to mass diffusivity. A considerable value of Sc shows no impact on the temperature plot. Figure 9 illustrates the Prandtl number (Pr) impact on the velocity, temperature, and concentration plot. An increase in Pr causes the velocity and temperature plot to degenerate. The Prandtl number explains the relationship between kinematic viscosity and thermal conductivity. Pr is beneficial in coordinating the thickening of momentum alongside thermal layers in heat transport analysis. Physically, any fluid with a higher Pr possesses viscosity, which helps to reduce the hydrodynamics and thermal layer thickness by reducing the velocity and temperature plot. Thus, Pr is a suitable parameter for increasing the liquid flow rate of cooling. However, if Pr>1, the liquid is highly conducive. The effect of Pr on concentration has been detected to be negligible. Figure 10 illustrates the impact of thermal Grashof number (Gr) on concentration, temperature, and velocity plots. An upward increment in the velocity plot is detected as the value of Gr increases. Because of this, the thermal Grashof number acted like a buoyancy force on the fluid velocity alongside the hydrodynamic layer thickness. Buoyancy force describes the upward liquid force exerted on the liquid. Thus, experimentally, pressure hikes the depth.

Furthermore, the bottom pressure of the displaced object becomes much greater than the force it possesses at the top. This implies a net vertical force that elevates the velocity along with the entire hydrodynamic layer thickness. As shown in Figure 10, the effect of Gr on temperature and concentration is negligible. The impact of the mass Grashof number (Gm) on the velocity, concentration, and temperature plots is illustrated in Figure 11. Gm is found to be significant on the velocity plot but negligible on the temperature and concentration plots. This indicates that the mass Grashof number behaves like a mass buoyancy effect. In Figure 12, an incremental value of the chemical reaction parameter (kr) is discovered to degenerate the velocity alongside the concentration plot. Practically, the chemical reaction term alters the species concentration by degenerating the solutal layer thickness. This indicates a destructive reaction in the fluid flow regime. Finally, the impact of Eckert number (Ec) is detected to elevate the velocity alongside the temperature plot in Figure 13. Physically, the Eckert number is derived from the viscous dissipation added to the energy Eq. (8). The Eckert number describes the relationship between the enthalpy in the flow and its kinetic energy. High values of Ec elevate the shear forces in the liquids.

Experimentally, heat energy is stored in the fluids due to frictional heating and elevating the thermal and hydrodynamic layers.

Table 1 shows the computational values for skin friction coefficient, Nusselt number (Nu), and Sherwood number (Sh) for encountered flow parameters. An increase in We is found to enhance the local skin friction and has a negligible effect on Sherwood and Nusselt numbers. A higher M value is detected, indicating that the local skin friction has degenerated. An incremental value of Gr and Gm is found to increase skin friction, but it has no effect on the Nusselt and Sherwood numbers. An increase in R enhances the hydrodynamic and thermal layer thickness by enhancing the skin friction and Nusselt number. A higher value of Pr is found to lessen the skin friction and elevate the Nusselt number.

On the other hand, a higher value of Ec is found to increase skin friction and lower the Nusselt number. An increase in the values of Du and So is found to accelerate the skin friction, while both effects are alternate on the Nusselt and Sherwood numbers. An increase in the values of Sc and kr is found to decelerate skin friction and elevate the Sherwood number. The skin friction and Nusselt number are observed to increase dramatically as the heat generation parameter is increased. In Table 2, an increase in the Dufour parameter is observed to increase the skin friction but decrease the rate of heat transfer by lowering the Nusselt number. A considerable value of the heat generation parameter is observed to increase the local Nusselt number and speed up the rate of heat transfer. A higher value of both the Schmidt number and the chemical reaction parameter is observed to decrease the local skin friction but speed up the rate of mass transfer. A considerable value of the Soret number increases the local skin friction but lowers the rate of mass transfer.

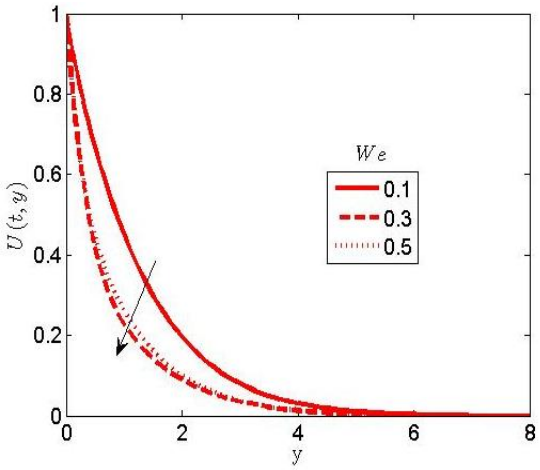

Fig. 3. The effect of the Weissenberg number on velocity plot

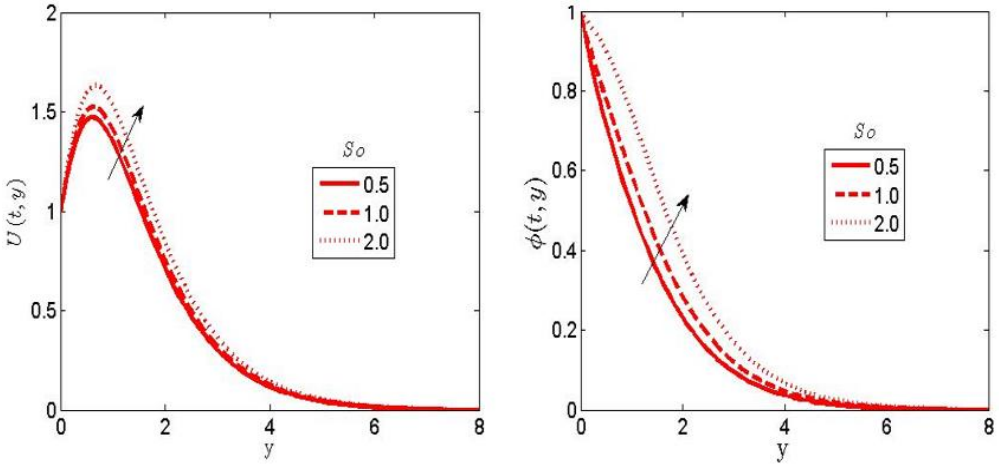

Fig. 4. The effect of the Soret term on the velocity, and concentration plots

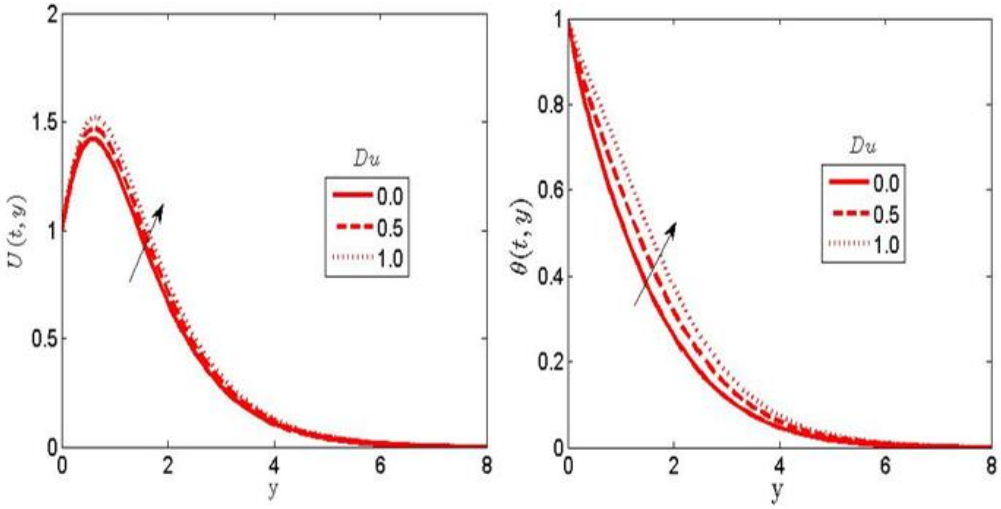

Fig. 5. The effect of the Dufour term on velocity, and temperature plots

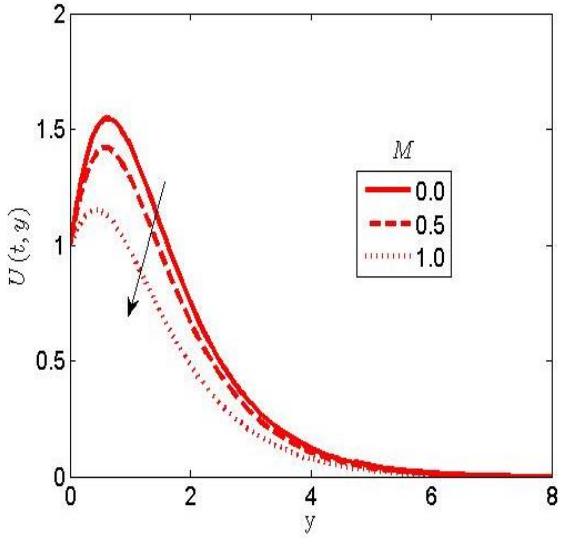

Fig. 6. The effect of the magnetic parameter on the velocity plot

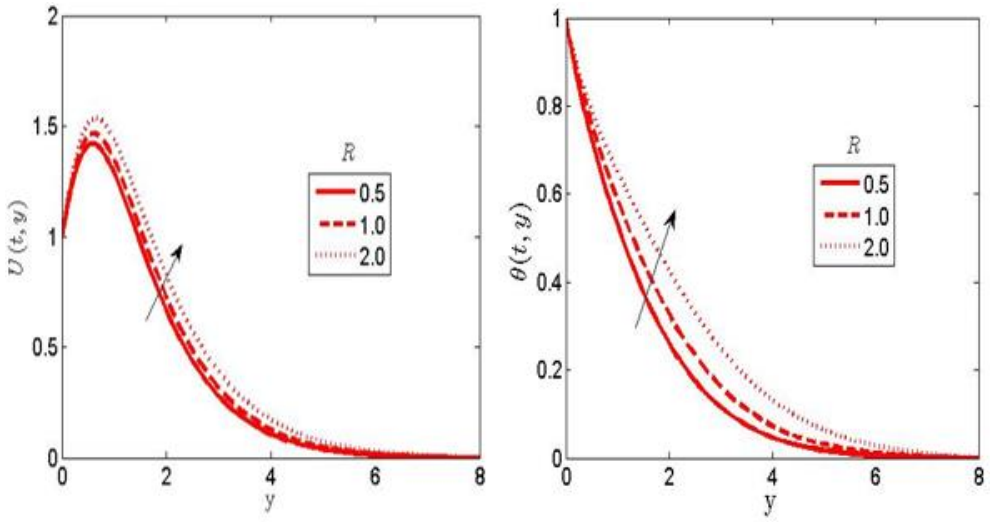

Fig. 7. The effect of the thermal radiation term on the velocity, and temperature plots

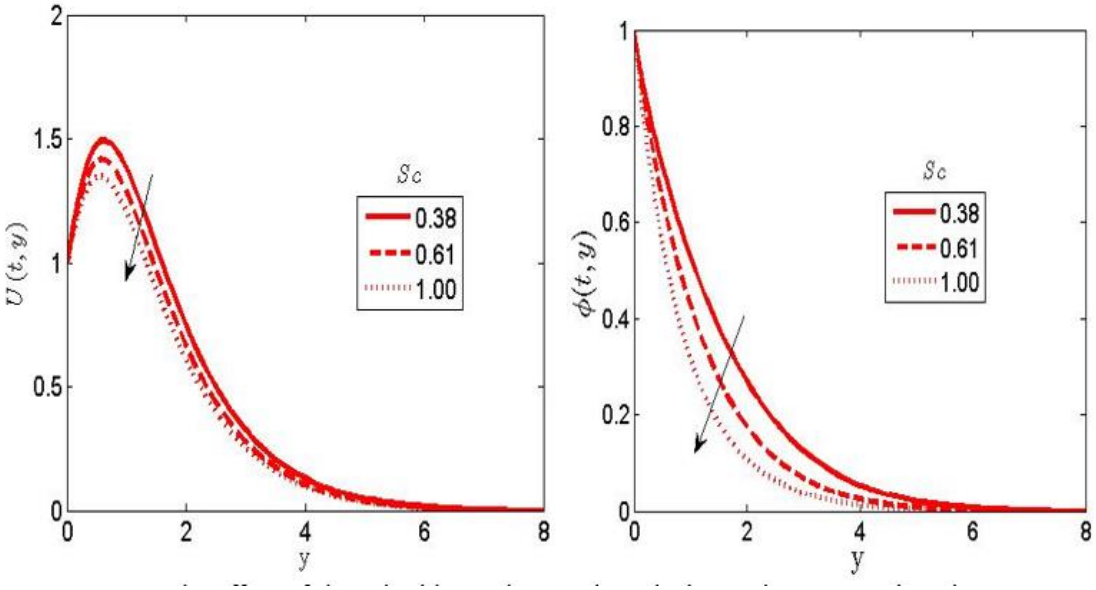

Fig. 8. The effect of the Schmidt number on the velocity, and concentration plots

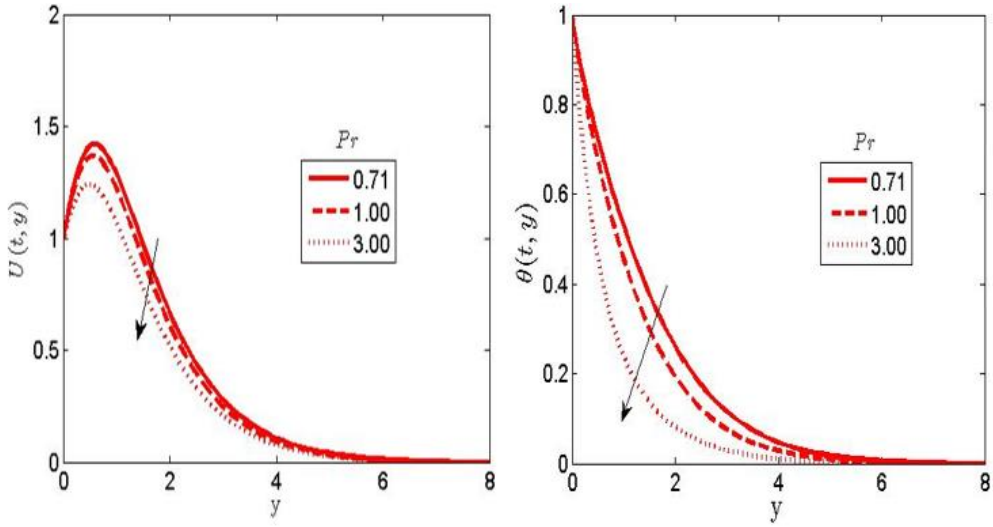

Fig. 9. The effect of the Prandtl number on velocity, and temperature plots

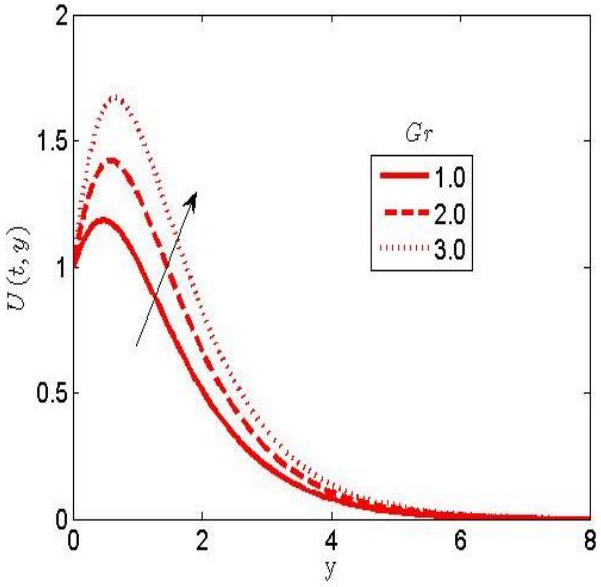

Fig. 10. The effect of the thermal Grashof number on the velocity plot

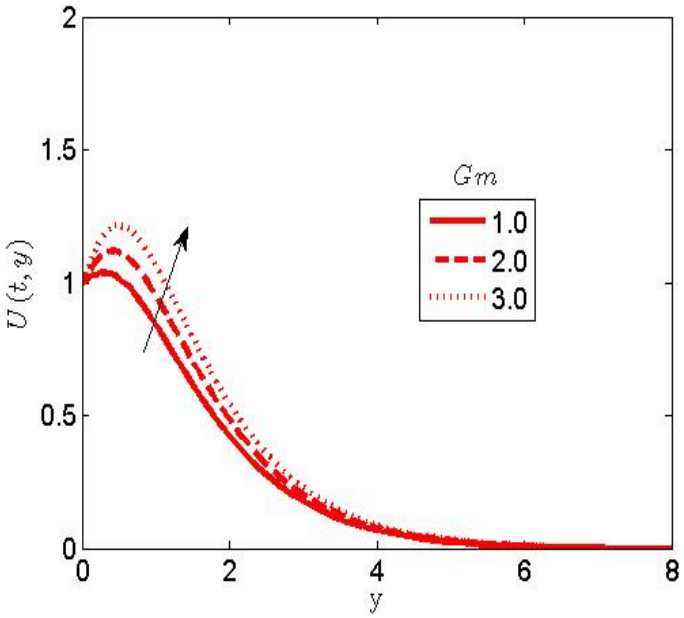

Fig. 11. The effect of the mass Grashof number on the velocity, temperature, and concentration plot

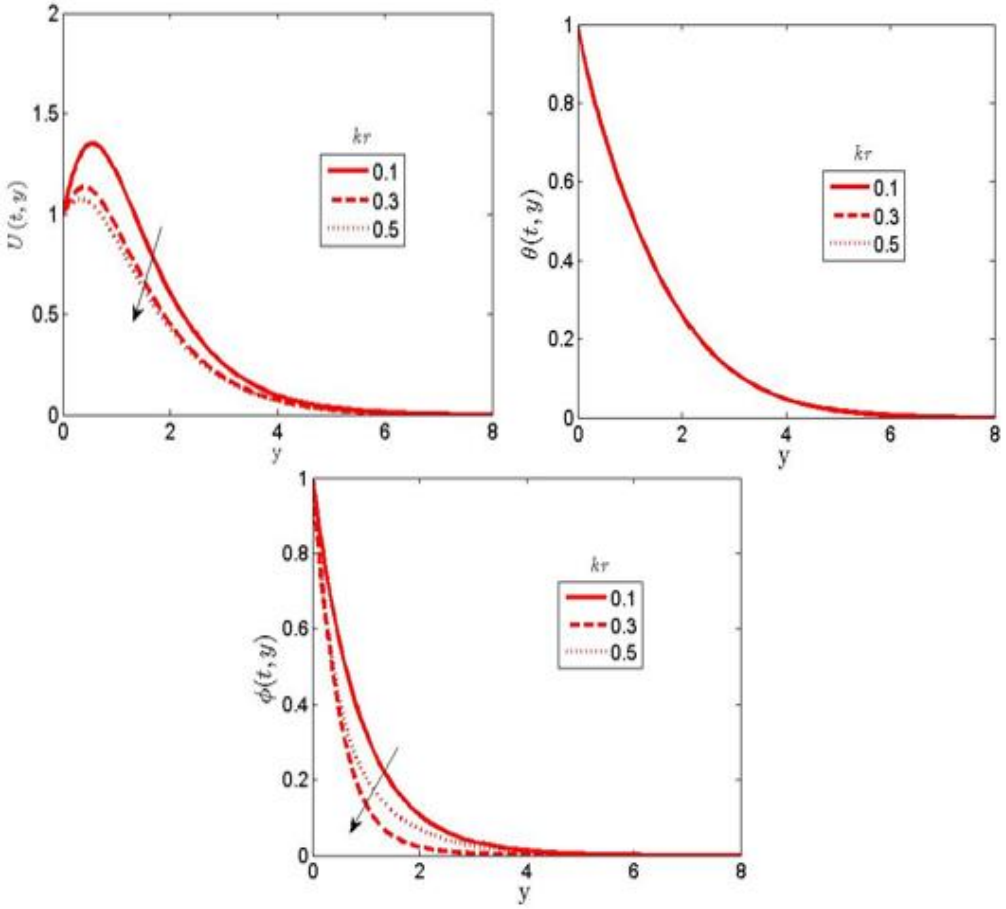

Fig. 12. The effect of the chemical reaction term on the velocity, temperature, and concentration plots

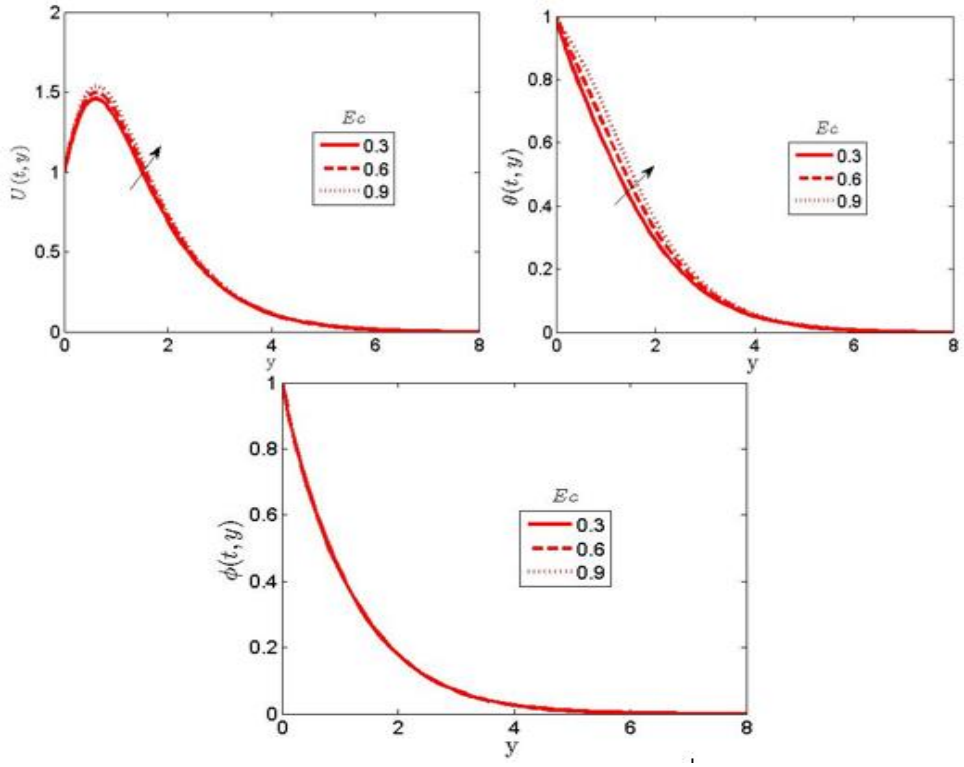

Fig. 13. The effect of the Eckert number on the velocity, temperature, and concentration plots

Table 1
Numerical values for skin friction coefficient(C_f), Nusselt number(Nu), and 180 herwood number (Sh) for different values of We, M, Gr, Gm, R, Pr and Ec

We	M	Gr	Gm	R	Pr	Ec	Cf	Nh	Sh
0.1							1.750914	0.527259	0.846371
0.3							1.471465	0.527259	0.846371
0.5							0.697697	0.527259	0.846371
	0.0						0.874356	0.600124	0.819900
	0.5						0.703415	0.600124	0.819900
	1.0						0.697697	0.600124	0.819900
		1.0					1.492511	0.511721	0.421001
		2.0					2.110665	0.511721	0.421001
		3.0					2.728819	0.511721	0.421001
			1.0				3.046706	1.812400	1.999900
			2.0				4.132881	1.812400	1.999900
			3.0				5.219055	1.812400	1.999900
				0.5			1.084532	0.560012	0.811076
				1.0			1.511023	0.6299	0.811076
				2.0			1.676520	0.7459	0.811076
					0.71		0.795904	0.567059	0.703384
					1.00		0.573571	0.874814	0.703384
					3.00		0.448097	1.498064	0.703384
						0.3	1.619464	0.628843	0.738124
						0.6	1.868109	1.014639	0.738124
						0.9	2.116755	1.400436	0.738124

Table 2
Comparison of the present numerical results with the published work of Hussain *et al.,* (2017) solved using analytical approach. $Gr = Gm = Du = Sc = t = \delta_x = R = 0$

Pr	We	n	$\theta'(0)$	$\theta'(0)$
			Hussain *et al.,* (2017) Analytical solution (HAM)	The present outcomes Numerical solution (SRM)
0.1			0.3438	0.3440
0.3			0.4597	0.4500
0.5			0.7921	0.7926
	1.0		0.2568	0.2570
	2.0		0.2740	0.2742
	3.0		0.3043	0.3047
		1.0	2.1523	2.1525
		2.0	1.5129	1.5130
		3.0	0.8937	0.8940

5. Conclusion

The analysis of unsteady MHD tangent hyperbolic liquid flow past a semi-infinite upward plate with Joule heating and influences of Soret-Dufour, viscous dissipation, and thermal radiation has been scrutinized numerically. The Rosseland diffusion model has been employed on the simplified coupled nonlinear PDEs to check the behavior of radiative heat flux. The outcomes of the present analysis are obtained by utilizing SRM. SRM is expressed in Lagrange polynimials interpolation employed to decouple PDEs' decouple systems by employing a relaxation approach. The following final remarks are drawn from the outcomes:

i. The tangent hyperbolic fluid is considered. Due to the high viscosity in this fluid, an incremental value of the Weissenberg number is found to degenerate the velocity profile;
ii. The Soret term is added to the specie equation in the problem of heat and mass, and in this paper, an increase in the Soret term is found to elevate the velocity alongside the concentration profile;
iii. By increasing the Dufour term, it is found that the speed along the temperature plot goes up;
iv. A magnetic field of uniform strength is imposed in the direction of the non-Newtonian fluid flow. Hence, the transverse magnetism is found to increase the strength of the Lorentz force as the velocity profile degenerates; and
v. We find that as the Schmidt number goes up, the velocity along the concentration plot goes down.

The outcomes of this study would be helpful in drilling operations, polymer engineering, and bioengineering. Because of the MHD nature of the liquid, this outcome is of interest in controlling magnetized metal welding and coating of metals. The outcomes of this study would also be helpful in separating isotopes.

The present exploration is expected to be helpful in the following fields:

i. This study will be of help in reducing the turbulence of blood flow due to magnetism;
ii. This study will be helpful in treating blood cancer by applying electromagnetic radiation and
iii. This study will be helpful in moderating pores in pathological studies.

References

[1] Naseer, Muhammad, Muhammad Yousaf Malik, Sohail Nadeem, and Abdul Rehman. "The boundary layer flow of hyperbolic tangent fluid over a vertical exponentially stretching cylinder." *Alexandria engineering journal* 53, no. 3 (2014): 747-750. https://doi.org/10.1016/j.aej.2014.05.001

[2] Ullah, Zakir, and Gul Zaman. "*Lie group analysis of magnetohydrodynamic tangent hyperbolic fluid flow towards a stretching sheet with slip conditions*." *Heliyon* 3, no. 11 (2017). https://doi.org/10.1016/j.heliyon.2017.e00443

[3] Subba Rao, Munagala Venkata, Kotha Gangadhar, and Giulio Lorenzini. "A computational analysis for boundary layer flow of magneto hydrodynamic tangent hyperbolic fluid of heat and mass transfer past a stretching cylinder with suction/injection using spectral relaxation method." *Mathematical Modelling of Engineering Problems* 6, no. 1 (2019). https://doi.org/10.18280/mmep.060105

[4] Mahdy, A., and G. A. Hoshoudy. "Two-phase mixed convection nanofluid flow of a dusty tangent hyperbolic past a nonlinearly stretching sheet." *Journal of the Egyptian Mathematical Society* 27, no. 1 (2019): 1-16. https://doi.org/10.1186/s42787-019-0050-9

[5] Abbas, M. Ali, Y. Q. Bai, M. M. Bhatti, and M. M. Rashidi. "Three dimensional peristaltic flow of hyperbolic tangent fluid in non-uniform channel having flexible walls." *Alexandria Engineering Journal* 55, no. 1 (2016): 653-662. https://doi.org/10.1016/j.aej.2015.10.012

[6] Falodun, B. O., and E. O. Ige. "Linear and quadratic multiple regressions analysis on magneto-thermal and chemical reactions on the Casson-Williamson nanofluids boundary layer flow under Soret-Dufour mechanism." *Arab Journal of Basic and Applied Sciences* 29, no. 1 (2022): 269-286. https://doi.org/10.1080/25765299.2022.2115688

[7] Alao, F. I., A. I. Fagbade, and B. O. Falodun. "Effects of thermal radiation, Soret and Dufour on an unsteady heat and mass transfer flow of a chemically reacting fluid past a semi-infinite vertical plate with viscous dissipation." *Journal of the Nigerian mathematical Society* 35, no. 1 (2016): 142-158. https://doi.org/10.1016/j.jnnms.2016.01.002

[8] Reddy, P. Bala Anki. "Magnetohydrodynamic flow of a Casson fluid over an exponentially inclined permeable stretching surface with thermal radiation and chemical reaction." *Ain Shams Engineering Journal* 7, no. 2 (2016): 593-602. https://doi.org/10.1016/j.asej.2015.12.010

[9] Hosseinzadeh, Kh, A. Jafarian Amiri, S. Saedi Ardahaie, and D. D. Ganji. "Effect of variable lorentz forces on nanofluid flow in movable parallel plates utilizing analytical method." *Case studies in thermal engineering* 10 (2017): 595-610. https://doi.org/10.1016/j.csite.2017.11.001

[10] Ghadikolaei, S. S., Kh Hosseinzadeh, and D. D. Ganji. "Analysis of unsteady MHD Eyring-Powell squeezing flow in stretching channel with considering thermal radiation and Joule heating effect using AGM." *Case studies in thermal engineering* 10 (2017): 579-594. https://doi.org/10.1016/j.csite.2017.11.004

[11] Hayat, Tasawar, Rai Sajjad, Taseer Muhammad, Ahmed Alsaedi, and Rahmat Ellahi. "On MHD nonlinear stretching flow of Powell–Eyring nanomaterial." *Results in physics* 7 (2017): 535-543. https://doi.org/10.1016/j.rinp.2016.12.039

[12] Sarfo, Frederick Kwaku, Francis Amankwah, and Daniel Konin. "Computer Self-Efficacy among Senior High School Teachers in Ghana and the Functionality of Demographic Variables on Their Computer Self-Efficacy." *Turkish Online Journal of Educational Technology-TOJET* 16, no. 1 (2017): 19-31.

[13] Vijaya, N., Y. Hari Krishna, K. Kalyani, and G. V. R. Reddy. "Soret and radiation effects on an unsteady flow of a casson fluid through porous vertical channel with expansion and contraction." *Frontiers in Heat and Mass Transfer (FHMT)* 11 (2018). https://doi.org/10.5098/hmt.11.19

[14] Reddy, G. V. R., and Y. Hari Krishna. "Soret and dufour effects on MHD micropolar fluid flow over a linearly stretching sheet, through a non-darcy porous medium." *International Journal of Applied Mechanics and Engineering* 23, no. 2 (2018): 485-502. https://doi.org/10.2478/ijame-2018-0028

[15] Suneetha, K., S. M. Ibrahim, and G. V. Ramana Reddy. "A study on free convective heat and mass transfer flow through a highly porous medium with radiation, chemical reaction and soret effects." *Journal of Computational and Applied Research in Mechanical Engineering* 8, no. 2 (2019): 121-132.

[16] Idowu, A. S., and B. O. Falodun. "Variable thermal conductivity and viscosity effects on non-Newtonian fluids flow through a vertical porous plate under Soret-Dufour influence." *Mathematics and Computers in Simulation* 177 (2020): 358-384. https://doi.org/10.1016/j.matcom.2020.05.001

[17] Idowu, A. S., and B. O. Falodun. "Variable thermal conductivity and viscosity effects on non-Newtonian fluids flow through a vertical porous plate under Soret-Dufour influence." *Mathematics and Computers in Simulation* 177 (2020): 358-384. https://doi.org/10.1016/j.matcom.2020.05.001

[18] Fagbade, A. I., B. O. Falodun, and A. J. Omowaye. "MHD natural convection flow of viscoelastic fluid over an accelerating permeable surface with thermal radiation and heat source or sink: spectral homotopy analysis approach." *Ain Shams Engineering Journal* 9, no. 4 (2018): 1029-1041. https://doi.org/10.1016/j.asej.2016.04.021

[19] Sobamowo, M. G. "Combined effects of thermal radiation and nanoparticles on free convection flow and heat transfer of casson fluid over a vertical plate." *International Journal of Chemical Engineering* 2018 (2018). https://doi.org/10.1155/2018/7305973

[20] Ganesh Kumar, K., B. J. Gireesha, and R. S. R. Gorla. "Flow and heat transfer of dusty hyperbolic tangent fluid over a stretching sheet in the presence of thermal radiation and magnetic field." *International Journal of Mechanical and Materials Engineering* 13, no. 1 (2018): 1-11. https://doi.org/10.1186/s40712-018-0088-8

[21] Fagbade, Adeyemi Isaiah, Bidemi Olumide Falodun, and Chika Uchechukwu Boneze. "Influence of magnetic field, viscous dissipation and thermophoresis on Darcy-Forcheimer mixed convection flow in fluid saturated porous media." *American Journal of Computational Mathematics* 5, no. 01 (2015): 18-40. https://doi.org/10.4236/ajcm.2015.51002

[22] Daniel, Yahaya Shagaiya. "Laminar convective boundary layer slip flow over a flat plate using homotopy analysis method." *Journal of The Institution of Engineers (India): Series E* 97 (2016): 115-121. https://doi.org/10.1007/s40034-016-0084-6

[23] Shahzad, F., M. Sagheer, and S. Hussain. "MHD tangent hyperbolic nanofluid with chemical reaction, viscous dissipation and Joule heating effects." *AIP advances* 9, no. 2 (2019). https://doi.org/10.1063/1.5054798

[24] Shahzad, Faisal, Wasim Jamshed, Tanveer Sajid, Kottakkaran Sooppy Nisar, and Mohamed R. Eid. "Heat transfer analysis of MHD rotating flow of Fe3O4 nanoparticles through a stretchable surface." *Communications in Theoretical Physics* 73, no. 7 (2021): 075004. https://doi.org/10.1088/1572-9494/abf8a1

[25] Hussain, Arif, M. Y. Malik, T. Salahuddin, A. Rubab, and Mair Khan. "Effects of viscous dissipation on MHD tangent hyperbolic fluid over a nonlinear stretching sheet with convective boundary conditions." *Results in physics* 7 (2017): 3502-3509. https://doi.org/10.1016/j.rinp.2017.08.026

[26] Ayegbusi, Florence D., Cletus Onwubuoya, and Bidemi O. Falodun. "Unsteady problem of magnetohydrodynamic heat plus mass transfer convective flow over a moveable plate with effects of thermophoresis and thermal radiation." *Heat Transfer* 49, no. 6 (2020): 3593-3612. https://doi.org/10.1002/htj.21790

[27] Jabeen, K., M. Mushtaq, and R. M. Akram Muntazir. "Analysis of MHD fluids around a linearly stretching sheet in porous media with thermophoresis, radiation, and chemical reaction." *Mathematical Problems in Engineering* 2020 (2020): 1-14. https://doi.org/10.1155/2020/9685482

[28] Anjum, Aisha, Sadaf Masood, Muhammad Farooq, Naila Rafiq, and Muhammad Yousaf Malik. "Investigation of binary chemical reaction in magnetohydrodynamic nanofluid flow with double stratification." *Advances in Mechanical Engineering* 13, no. 5 (2021): 16878140211016264. https://doi.org/10.1177/16878140211016264

[29] Abo-zaid, Omima A., R. A. Mohamed, F. M. Hady, and A. Mahdy. "MHD Powell–Eyring dusty nanofluid flow due to stretching surface with heat flux boundary condition." *Journal of the Egyptian Mathematical Society* 29, no. 1 (2021): 1-14. https://doi.org/10.1186/s42787-021-00123-w

[30] Yadav, Pramod Kumar, and Amit Kumar Verma. "Analysis of immiscible Newtonian and non-Newtonian micropolar fluid flow through porous cylindrical pipe enclosing a cavity." *The European Physical Journal Plus* 135 (2020): 1-35. https://doi.org/10.1140/epjp/s13360-020-00672-6

[31] Hussain, Azad, Mubashar Arshad, Ali Hassan, Aysha Rehman, Hijaz Ahmad, Jamel Baili, and Tuan Nguyen Gia. "Heat transport investigation of engine oil based rotating nanomaterial liquid flow in the existence of partial slip effect." *Case Studies in Thermal Engineering* 28 (2021): 101500. https://doi.org/10.1016/j.csite.2021.101500

[32] Dawar, Abdullah, Zahir Shah, Hashim M. Alshehri, Saeed Islam, and Poom Kumam. "Magnetized and non-magnetized Casson fluid flow with gyrotactic microorganisms over a stratified stretching cylinder." *Scientific Reports* 11, no. 1 (2021): 16376. https://doi.org/10.1038/s41598-021-95878-8

[33] Falodun, B. O., A. A. Ayoade, and O. Odetunde. "Positive and negative soret and dufour mechanism on unsteady heat and mass transfer flow in the presence of viscous dissipation, thermal and mass buoyancy." *Australian Journal of Mechanical Engineering* 21, no. 3 (2023): 965-978. https://doi.org/10.1080/14484846.2021.1938950

[34] Falodun, Bidemi O., C. Onwubuoya, and FH Awoniran Alamu. "Magnetohydrodynamics (MHD) heat and mass transfer of Casson fluid flow past a semi-infinite vertical plate with thermophoresis effect: spectral relaxation analysis." In *Defect and Diffusion Forum*, vol. 389, pp. 18-35. Trans Tech Publications Ltd, 2018. https://doi.org/10.4028/www.scientific.net/DDF.389.18

[35] Hussain, Azad, Ali Hassan, Qasem Al Mdallal, Hijaz Ahmad, Aysha Rehman, Mohamed Altanji, and Mubashar Arshad. "Heat transport investigation of magneto-hydrodynamics (SWCNT-MWCNT) hybrid nanofluid under the thermal radiation regime." *Case Studies in Thermal Engineering* 27 (2021): 101244. https://doi.org/10.1016/j.csite.2021.101244

[36] Hussain, Azad, Mubashar Arshad, Aysha Rehman, Ali Hassan, S. K. Elagan, Hijaz Ahmad, and Amira Ishan. "Three-dimensional water-based magneto-hydrodynamic rotating nanofluid flow over a linear extending sheet and heat transport analysis: A numerical approach." *Energies* 14, no. 16 (2021): 5133. https://doi.org/10.3390/en14165133

[37] Idowu, A. S., and B. O. Falodun. "Soret–Dufour effects on MHD heat and mass transfer of Walter'sB viscoelastic fluid over a semi-infinite vertical plate: spectral relaxation analysis." *Journal of taibah university for science* 13, no. 1 (2019): 49-62. https://doi.org/10.1080/16583655.2018.1523527

[38] Motsa, S. S. "New iterative methods for solving nonlinear boundary value problems." In *Fifth Annual Workshop on Computational Applied Mathematics and Mathematical Modeling in Fluid Flow*, pp. 9-13. Pietermaritzburg, South Africa: School of Mathematics, statistics and computer science, Pietermaritzburg Campus, 2012.